Chapter

Applications of Infrared Thermography for Non-destructive Characterization of Concrete Structures

Ravibabu Mulaveesala, Geetika Dua and Vanita Arora

Abstract

Usage of reinforced concrete structures has very long tradition in infrastructure industry due to their low cost, high strength, robustness, sustainability along with the easy availability of raw materials. However, they also have some drawbacks such as poor tensile strength and ductility, which leads to the formation of cracks in the structures. These cracks may cause penetration of chlorides, resulting into corrosion in the reinforcement. Quality control, maintenance and planning for the restoration of these structures demands a suitable non-destructive testing and evaluation method for wide-area monitoring to detect the hidden corrosion of the rebar at an early stage. Infrared thermal wave imaging has emerged as a viable technique for non-destructive testing and evaluation of reinforced concrete structures due to its full-field, remote, fast inspection capabilities to monitor the sub-surface rebar corrosion. Among the various thermal non-destructive testing techniques the present chapter proposes a novel aperiodic thermal wave imaging technique named as Gaussian windowed frequency modulated thermal wave imaging for testing and evaluation of rebar corrosion in concrete structures.

Keywords: concrete structures, frequency modulation, image processing, matched filter, non-destructive testing, phase images, pulse compression, rebar, thermal non-destructive testing, thermal wave imaging

1. Introduction

Reinforced concrete is a durable material, capable of bearing various severe environmental conditions. It is an extensively used material for constructing bridges, buildings, flyovers and underground structures. Despite of the fact that majority of these structures have high strength, durability and show good long term performance, there are large number of failures of concrete structures as a result of premature corrosion in reinforcement. The main reasons behind the corrosion initiation of reinforcing steel are the ingress of chloride ions and carbon dioxide to the steel surface, leading to the significant loss in cross-section. During the corrosion process, iron oxides and hydroxides being the corrosion products are usually get deposited in the concrete around the steel material. Their formation within this confined space sets up stress, which crack and spall the concrete cover. This, in

turn, results in progressive deterioration of the concrete. As a result, repair costs constitute a major part of spending on infrastructure. There have been a large number of investigations on the problems of deterioration of concrete and the consequent corrosion of rebar. It is essential to monitor the state of such deliberate structures right from the construction stage by carrying out periodic inspections and thus maintaining record of the results. For the estimation of corrosion rate of reinforced steel in concrete, many electrochemical and non-destructive techniques are available.

Non-destructive testing and evaluation (NDT&E) is defined as the application of an inspection method to assess the integrity of the object without impairing its future usefulness [1]. Non-destructive testing (NDT) plays a crucial role in various applications to inspect the quality and safety of the products in a reliable and cost effective manner [1–12].

Widely used NDT&E methods can be broadly classified based on their applicability as point-wise or whole-field techniques. In point-wise methods, the test specimen is scanned on each and every point in order to reveal information regarding the hidden defects, whereas, whole-field methods provide full information of the test specimen in a single run. Depending upon the way, the test is going to be implemented i.e. the specimen to be tested is in contact with the test unit or it can be tested remotely, these NDT&E techniques can be sub-classified as contact or non-contact techniques. Further, depending on the capability of the technique to be adopted for NDT&E, these techniques can be classified as surface, sub-surface or volumetric techniques [3–20]. In view of their merits, always whole-field, non-contact and volumetric NDT&E techniques are preferable over the others. Infrared thermography (IRT) is a well-established tool in the field of non-destructive testing and evaluation [13–21].

2. Infrared thermography

Infrared thermography is based on the fact that all objects above 0 K temperature, emits infrared energy as a function of their temperature. Infrared radiation corresponds to the band of the electromagnetic spectrum that lies in between 0.74 and 1000 μm wavelength region (as shown in **Figure 1**).

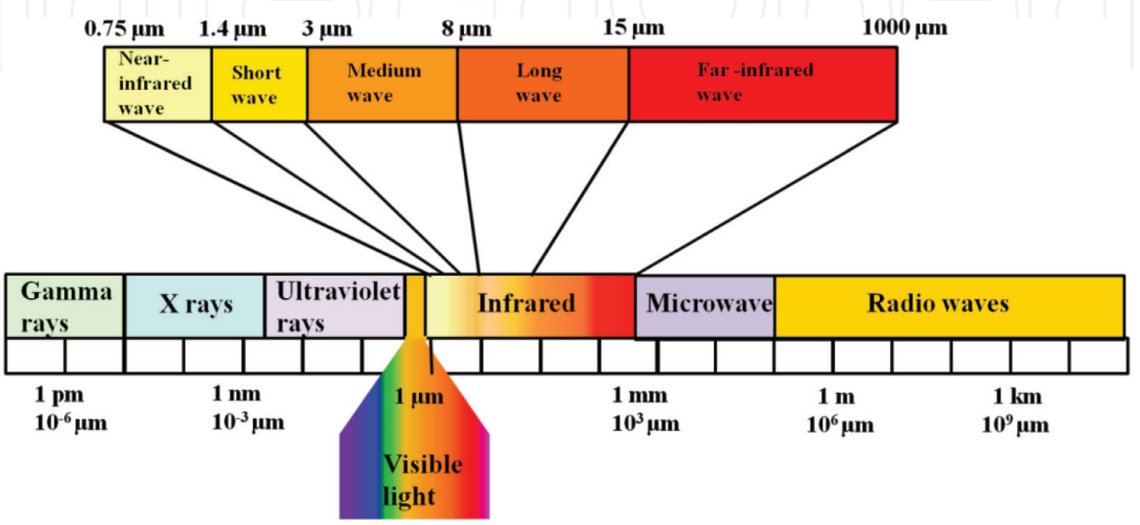

Figure 1.
Electromagnetic spectrum.

The emitted radiation at each and every wavelength and the corresponding temperature distributions for a given object is explained from the Wien's law. It states that hotter objects emit most of their radiation at shorter wavelengths whereas colder objects emit at longer wavelengths. It is as illustrated in **Figure 2**.

According to Stefan-Boltzmann law, the net radiated power per unit area is proportional to the fourth power of object's temperature as mentioned below [1]:

$$P = \varepsilon\sigma T^4 \tag{1}$$

where P is the net radiated power per unit area [W/m^2], ε is emissivity, σ is Stefan-Boltzmann constant [5.6703 × 10^{-8} W/m^{2}K^4] and T is temperature [K].

IRT can be defined as a technique which detects the infrared radiation emanating by an object, converts it into temperature and displays into an image named as thermogram. It is a fast, remote, whole-field and quantitative characterization technique which provides real-time information. It can be applied to inspect various materials and have numerous applications in various fields such as structural health monitoring (SHM), non-destructive testing, quality inspection in metal or non-metal materials such as alloys or composites, civil engineering and building sciences.

IRT for SHM/NDT&E applications involves mapping of the temperature over the structure/specimen for characterizing its surface and sub-surface structural defects. The surface of the test specimen is illuminated using heat sources and infrared camera is used to map the resultant temperature profile over the specimen. Further, the recorded temperature distribution is processed and analyzed to produce thermal images. IRT has gained wide acceptance and plays a crucial role in the field of testing and evaluation due to its merits such as non-contact, whole-field, safe and fast inspection capabilities for characterization of various materials irrespective of their electrical, optical and magnetic properties.

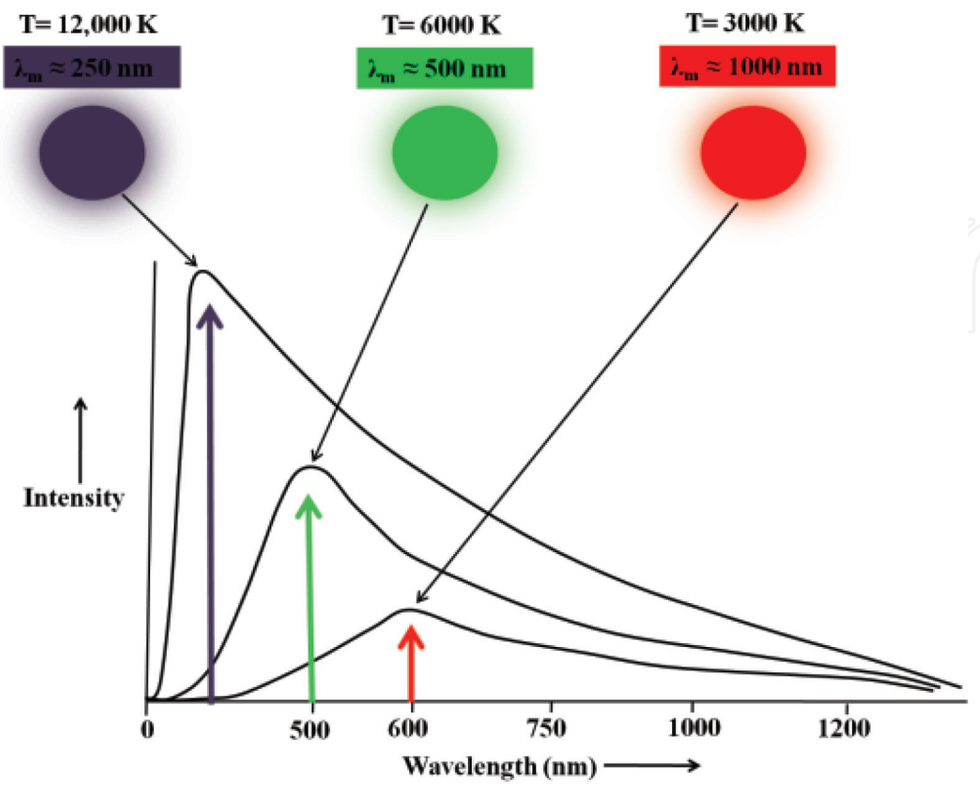

Figure 2.
Illustration of Wein's law.

IRT can be implemented in two ways: passive and active. In passive approach, the test specimen or the structure is naturally at different temperature than the ambient i.e. the passive approach is used when the defective/faulty regions in the test specimen provides enough thermal contrast with respect to the sound (non-faulty) region. Typical applications of passive thermography includes seepage/moisture assessment, insulation problems in buildings, condition monitoring, structural health monitoring, etc. However, due to the limited depth of penetration and inability in providing the quantitative assessment for the sub-surface defects deep inside the test specimen, restricts its applicability for NDT&E applications [13–21].

On contrary, to detect defects located deep inside the test specimen/stress concentration points inside the structure with enough thermal contrast, active thermography is preferred. In active approach, an external heat stimulus with a predefined amplitude, duration and bandwidth is imposed onto the test specimen. These known characteristics of the external thermal stimulus, helps in providing quantitative estimation of the sub-surface defects.

2.1 Widely used active IRT techniques for testing and evaluation of concrete structures

Active IRT (AIRT) has been developed as a non-destructive testing technique to detect surface and sub-surface defects by monitoring the emitted thermal radiations over the test object in response to a predefined applied excitation. A typical experimentation used to carry out AIRT is as shown in **Figure 3**.

AIRT is an emerging technique that has the potential to provide quantitative information about the hidden defects in a limited span of time. Based on the employed excitation scheme, AIRT can be classified as pulsed and modulated thermographic methods. Pulse thermography (PT) [3–9] and pulse phase thermography (PPT) [11, 12] are the two pulse based thermographic methods.

In PT, the test specimen is excited using a short duration high peak power pulse and the corresponding temporal temperature distribution is monitored. The main advantage of the PT approach is its fast implementation. In general, the results obtained with this technique are based on the raw temperature profile obtained over the test specimen. The obtained thermal data is not only influenced by the sub-surface defects inside the test structure but also affected by the emissivity as well as non-uniform illumination variations over it. These artifacts may lead in bringing difficulties in interpretation of test results. In addition to these, the requirement of

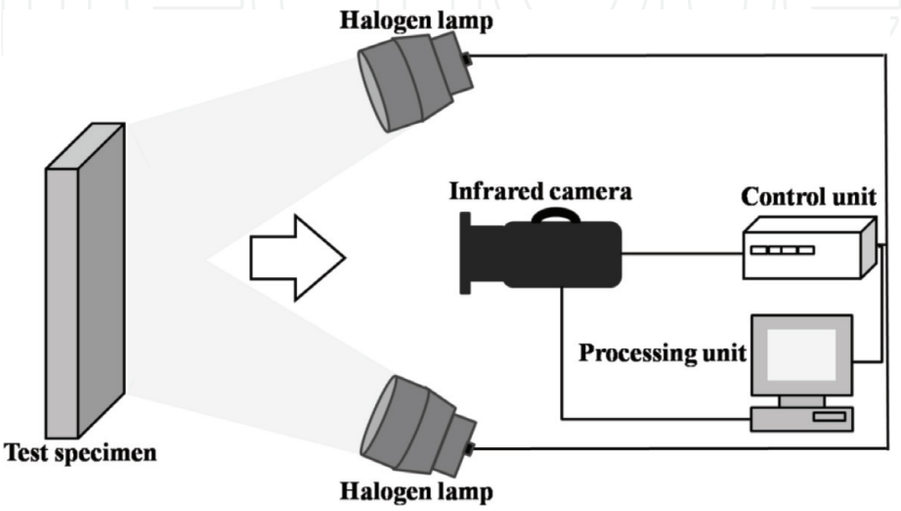

Figure 3.
Experimental set up.

high peak power heat sources to probe high frequency thermal waves into the test specimen (to resolve defects located inside the test specimen at various depths of different lateral dimensions) limits its applicability as far as the experimental setup cost is concerned.

Experimentation involved in pulse phase thermography is similar to PT (i.e. the test specimen is excited with a short duration high peak power pulse and the temperature variation over the surface of the structure is captured using an infrared camera) but it differs from the involved post-processing on the captured temporal temperature distribution. In this, the captured thermal distribution is analyzed in frequency domain using discrete Fourier transform (DFT) to extract the phase and magnitude information from its transformed temperature distribution. Phasegrams are of particular interest in non-destructive evaluation, as phase is less affected by environmental reflections, emissivity variations and non-uniform heating than that of the raw thermal data. This phase information plays a crucial role not only for qualitative representation in identifying the sub-surface defects but also helps in providing quantitative details. In addition to its fast inspection capabilities, results obtained with this technique are less sensitive to surface features of the object such as emissivity variations and non-uniform illuminations [11]. Even though, it has above mentioned merits still the requirement of high peak power heat sources limits its applicability [14].

In order to overcome the requirement of high peak power heat sources, modulated thermographic techniques are introduced by driving the heat sources at a predefined frequency, decided by the sample thickness and its thermal properties. In general, this modulation is carried out by a single frequency to provide thermal stimulus onto the test specimen and is named as lock-in thermography (LT) [10]. In LT, a sinusoidal modulated heat flux is imposed onto the test specimen and the resultant temporal temperature distribution is captured during the active heating. Further, from the extracted temporal temperature response, the phase-grams are reconstructed either by implementing quadrature phase shift or by Fourier Transform approach. These reconstructed phase images not only have the advantages such as less sensitive to emissivity variations and non-uniform heating over the test specimen but also helps in deeper depth of probing inside the test specimen.

Even though, the technique allows detection of defects located deep inside the test specimen with moderate peak power heat sources, but the mono-frequency excitation limits its applicability in identifying defects located at various depths inside the test specimen with enough resolution. In order to detect defects located at different depths of various lateral dimensions with enough resolution, LT has to be carried out with different excitation frequencies. This makes LT a time-consuming testing technique. These limitations can be overcome by probing thermal waves with suitable band of frequencies having significant magnitude into the test sample in a single experimentation cycle with relatively low peak power sources. To achieve this, the present chapter focuses on one of the available aperiodic thermal wave imaging techniques i.e. linear frequency modulated thermal wave imaging. This technique is introduced to overcome the limitations (resolution, peak power, limited depth of penetration) of the conventional (PT, PPT, LT) thermographic techniques.

2.2 Gaussian windowed frequency modulated thermal wave imaging

This present chapter highlights the capabilities of aperiodic linear frequency modulated thermal wave imaging (LFMTWI) and the associated post-processing techniques for detection of corrosion in rebar [18–21]. In LFMTWI, the surface of the test specimen is heated by driving the heat sources with a linear frequency modulated heat flux, which results into a similar frequency modulated temperature distribution over it, with a mean rise in temperature depending on the total

duration of the excitation. This helps in probing the desired band of thermal waves (decided by thermal properties of the test specimen, location and spatial dimensions of the defects) with significant magnitude in a limited time span into the test specimen which improves defect detection resolution.

However, smaller ratio of the concentration of the supplied energy in the main lobe to that of side lobe levels of the compressed pulse obtained from the matched filtering processing limits its defect detection resolution and sensitivity. The present chapter highlights the concept of spectral reshaping considered for proposed LFMTWI, in order to improve the pulse compression properties which lead to enhance the defect detection resolution and sensitivity. It is incorporated by reshaping the captured temporal thermal distribution obtained from LFMTWI experimentation using a Gaussian window and is named as Gaussian windowed frequency modulated thermal wave imaging (GWFMTWI). Further, the capabilities of GWFMTWI for detection of corrosion in reinforced rebar are compared with LFMTWI considering signal to noise ratio (SNR) as a figure of merit.

3. Theory

In LFMTWI, linear frequency modulated (LFM) heat flux is imposed onto the test sample to probe thermal waves into it. These thermal waves diffuse into the test sample by producing similar time varying temperature distributions over the surface except a mean rise during the dynamic heating. The theoretical model represented to study this thermal response can be derived from the one-dimensional heat diffusion equation given as [14]:

$$\frac{\partial^2 T(x',t')}{\partial^2 x'} - \frac{1}{\alpha}\frac{\partial T(x',t')}{\partial t'} = 0 \tag{2}$$

where α is the thermal diffusivity ($\alpha = k'/\rho.c$); ρ, c, k' are the density, specific heat and thermal conductivity of the medium respectively. $T(x',t')$ is the temperature response over the surface and x' is the spatial dimension in the direction of heat flow.

The proposed (frequency modulated) heat flux$Q(x',t')$ of duration τ [s], with a bandwidth B [Hz], is obtained by means of the LFM excitation signal used to drive the heat sources [14],

$$Q(x'=0,t') = Q_0 e^{2\pi j\left(f_0 t' + \frac{Bt'^2}{2\tau}\right)} \tag{3}$$

where Q_0 is the envelope of the frequency modulated incident heat flux (chirp signal), which is zero outside the time interval τ [s], f_0 is the initial frequency [Hz] and $2\pi j\left(f_0 t' + \frac{Bt'^2}{2\tau}\right)$ is the phase of the LFM (chirp) incident heat flux.

The solution to heat equation (Eq. (2)) for a LFM heat flux (Eq. (3)) over the test specimen by considering it as a semi-infinite solid with specified boundary ($x' = 0$, a similar kind of temperature response is expected and $x' \to \infty$, ambient temperature) and initial conditions ($T(x', t' = 0) = 0$)) is obtained as [14]:

$$\begin{aligned} T(x',t') = {} & T_0 e^{2\pi j\left(f_0 t' + \frac{Bt'^2}{2\tau}\right)} e^{-x'\sqrt{\frac{\pi}{\alpha}\left(f_0 + \frac{Bt'}{\tau}\right)}} e^{-jx'\sqrt{\frac{\pi}{\alpha}\left(f_0 + \frac{Bt'}{\tau}\right)}} \\ & - \frac{2T_0}{\sqrt{\pi}} e^{2\pi j\left(f_0 t' + \frac{Bt'^2}{2\tau}\right)} \int_0^{x'/2\sqrt{\alpha t'}} e^{\frac{-\pi j x'^2}{2\alpha\mu^2}\left(f_0 + \frac{Bt'}{\tau}\right)} e^{-\mu^2} d\mu \end{aligned} \tag{4}$$

The second term in Eq. (4) is a transient disturbance caused by starting oscillations of surface temperature at initial time. It dies away as t' increases, leaving the first term which is a steady-state solution i.e.

$$T(x',t') = T_0 e^{2\pi j\left(f_0 t' + \frac{Bt'^2}{2\tau}\right)} e^{-x'\sqrt{\frac{\pi}{\alpha}\left(f_0+\frac{Bt'}{\tau}\right)}} e^{-jx'\sqrt{\frac{\pi}{\alpha}\left(f_0+\frac{Bt'}{\tau}\right)}} \tag{5}$$

where B/τ is the modulation factor and τ is duration of excitation. The thermal diffusion length μ [m] from the above solution (Eq. (5)) can be derived as [14]:

$$\mu = \sqrt{\frac{\alpha}{\pi\left(f_0 + \frac{Bt'}{\tau}\right)}} \tag{6}$$

Thus, it can be justified from Eq. (6) that LFMTWI ensures depth scanning of the sample with time in a single experimentation cycle.

In GWFMTWI technique, the envelope of the obtained solution for LFMTWI (Eq. (5)) is reshaped by using Gaussian window function given as in Eq. (7):

$$g(t') = e^{-\frac{(t'-\mu')^2}{2(\sigma')^2}} \tag{7}$$

where μ' and σ' are the mean and standard deviation respectively.

To facilitate the spectral reshaping on LFMTWI, the Fourier transform (FT) of $g(t')$,$(G(f))$ is multiplied with FT of the captured temporal temperature distribution at a given location $(T(x_i', f))$ over the test specimen and then converting it back to time domain using inverse Fourier transform (IFT). The obtained Gaussian windowed chirp (GWC) response (TGWC) can be represented as in Eq. (8):

$$T_{GWC/Gaussian} = \mathrm{IFT}(G(f).T(x_i',f)) \tag{8}$$

4. Results and discussion

To validate the proposed approach, a concrete sample of 6.7 cm thickness, containing 4 cm thickness mild steel rebar of length 13.24 cm is considered. The rebar is placed in sample by wounding a cotton cloth to fill up the groves in order to avoid incursion of concrete into the grooved area. A simulated corrosion has been introduced to the rebar by introducing four grove cuts of different widths (a, b, c and d) with a material loss of 5 mm from the surface of bar. The front view, side view and its experimental orientation is as shown in **Figure 4**. Further, experiments have been performed with LFMTWI technique on this sample. The experimental setup is shown in **Figure 5**.

A linear frequency modulated (LFM) signal with a frequency variation from 0.01 to 0.1 Hz at a sampling rate of 25 Hz of 100 s duration, is generated to drive the heat sources (two halogen lamps of each 1000 W/m^2) by the power control unit. During the active heating over the test structure for a frequency modulated incident heat flux, temporal temperature distribution over the test specimen is captured by an infrared camera (FLIR 5500) and images (thermograms) are captured at every 0.04 s time intervals for duration of 100 s. Further, temporal temperature distribution for each pixel is obtained from the thermal sequence and fitted with a linear fit. Post processing of the obtained data has been carried out after removing the mean rise of the thermal response for a given frequency modulated excitation for obtaining the dynamic variation in the temperature data. Next, Gaussian windowed (with mean 50 and standard deviation of 28) spectral reshaping have been

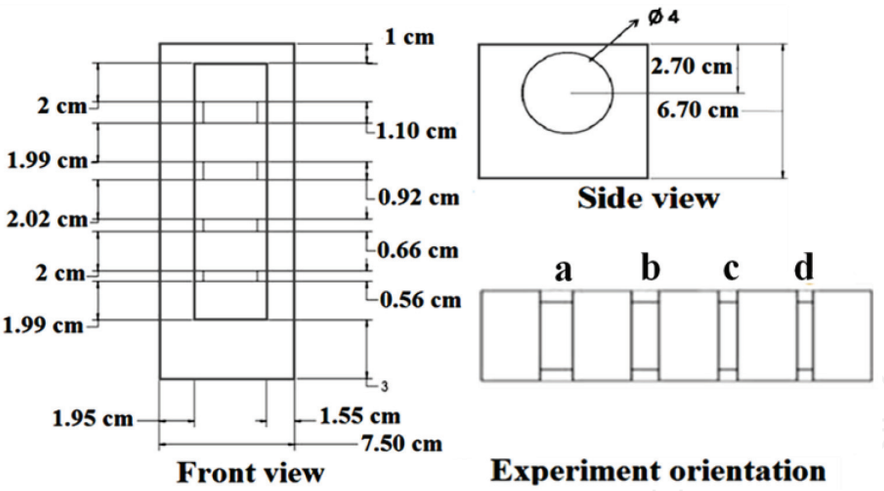

Figure 4.
Schematic of the experimental concrete sample.

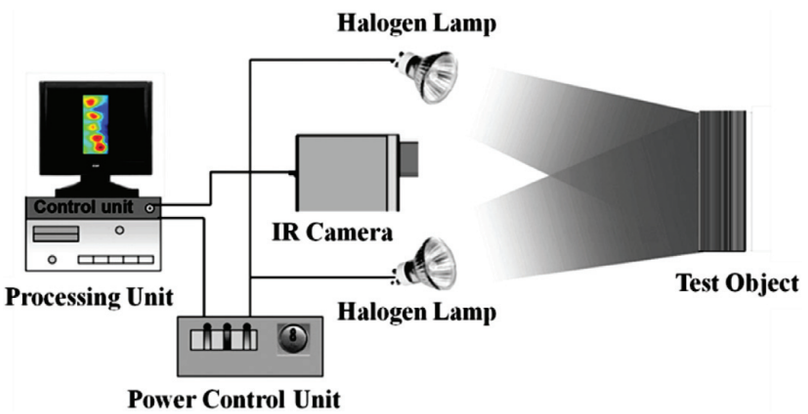

Figure 5.
Schematic of infrared imaging system used for experimentation.

performed onto the zero mean data to improve the pulse compression properties. Multi-transform techniques have been implemented both in time and frequency domain in order to compare sub-surface defect detection capabilities of these LFMTWI and GWFMTWI techniques. The conventional frequency domain amplitude (magnitude) and phase images are obtained by taking the FT of the Gaussian windowed temporal temperature data ($T_{Gaussian}(x, y, t)$), to the pixels in the field of view as below [2, 11, 19]:

$$T(x,y,k) = \sum_{n=0}^{N-1} T_{Gauusian}(x,y,t)e^{-\frac{j2\pi kn}{N}} = \mathrm{Re}(T(x,y,k)) + jImg(T(x,y,k)) \qquad (9)$$

where k is the bin number, N is total number of frames, $Re(T(x,y,k))$and $Img(T(x,y,k))$ are the real and imaginary parts of $T(x,y,k)$ respectively. Further, the magnitude images are reconstructed as [2, 11, 19]:

$$|T(x,y,k)| = \sqrt{(\mathrm{Re}(T(x,y,k)))^2 + (Img(T(x,y,k)))^2} \qquad (10)$$

and the phase images are reconstructed by using the equation as [2, 11, 19]:

$$\angle T(x,y,k) = \tan^{-1}\left(\frac{Img(T(x,y,k))}{\mathrm{Re}(T(x,y,k))}\right) \qquad (11)$$

The time domain matched filtering has been carried out in two different approaches, in the first a linear correlation approach has been implemented on the zero mean Gaussian temporal temperature distribution whereas in the later, a circular correlation approach has been adopted. The flowchart representing the pulse compression approach using linear correlation approach is as shown in **Figure 6**, whereas **Figure 7** represents the process for obtaining the pulse compression (PC) using circular correlation. Mathematically, pulse compression using linear correlation can be obtained as [13–19]:

$$T_{PC}(x,y,\tau') = \int_{-\infty}^{+\infty} T_{Gauusian}(x,y,t').T_{Reference}(x,y,(t'-\tau'))dt' \tag{12}$$

whereas, the pulse compression using circular correlation is obtained as:

$$T_{CCC}(x,y,t') = IFT\left\{FT\left(T_{Reference}(x,y,t')\right)^{*}.FT(T_{Gaussian}(x,y,t'))\right\} \tag{13}$$

The resultant images obtained after post processing are shown in **Figure 8**. The magnitude images obtained at a frequency of 0.02 Hz as a result of frequency domain analysis are as shown in **Figure 8(a)** using LFMTWI and (b) obtained for GWFMTWI. It's clear from the computed SNRs (as in **Table 1**) that the obtained frequency domain magnitude image from GWFMTWI technique is having better detection capabilities than that of the obtained frequency domain magnitude image for the FMTWI technique. Further, the reconstructed phase images at a frequency of 0.06 Hz and 6.84 Hz using LFMTWI and GWFMTWI techniques are as shown in **Figure 8(c)** and **(d)**, respectively. Unlike the facts mentioned in literature regarding the depth resolvability of the frequency domain phase images and their advantages and their merits over the magnitude images, the present studies over the concrete structures showed the magnitude images have better resolvability than that of the obtained phase grams to detect the corrosion of the rebar inside concrete structures. This is evident from the computed SNRs tabulated in **Table 1**.

The obtained pulse compressed correlation coefficient images reconstructed by the correlation approach for LFMTWI (at a time instant of 62.92 s) and GWFMTWI (at a time instant of 46.32 s) techniques are as shown in **Figure 8(e)** and **(f)** respectively. Due to the efficient pulse compression capabilities of the GWFMTWI technique, obtained linear correlation coefficient results shows the better SNR in comparison to that of LFMTWI technique. However, the time domain amplitude (correlation coefficient) images reconstructed from circular correlation approach (CCC) at a time instant of 56 s are as shown in **Figure 8(g)** and **(h)** obtained for LFMTWI and GWFMTWI techniques respectively. It is clear that the obtained results from the proposed CCC approach, proposed pulse compression approaches are far superior than that of the conventional frequency domain phase approach in order to detect the corrosion in rebar hidden inside the concrete structures.

It is observed from the results that the magnitude/correlation coefficient images shows their merits in comparison to that of the conventional frequency domain phase images in order to resolve the hidden corrosion of the rebar inside the concrete structures.

For quantitative comparison among the adopted multi-transform schemes SNR is taken as a figure of merit. The values of the SNRs are computed for the grove cuts (a, b, c and d) and the comparison has been made for various time and frequency domain multi-transform techniques with (LFM) and with spectral reshaping (GWFM) are tabulated in **Table 1** and also presented in the bar graph as shown in **Figure 9**.

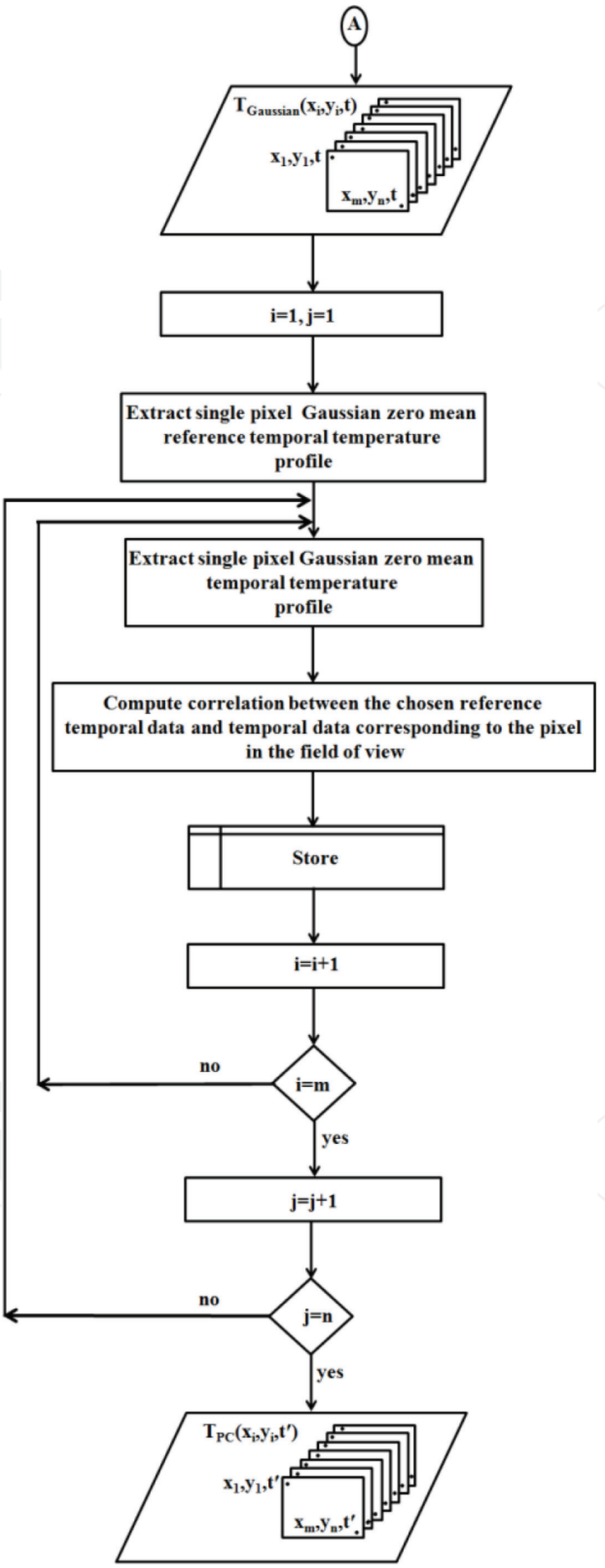

Figure 6.
Flow chart for obtaining pulse compression using linear correlation approach [19].

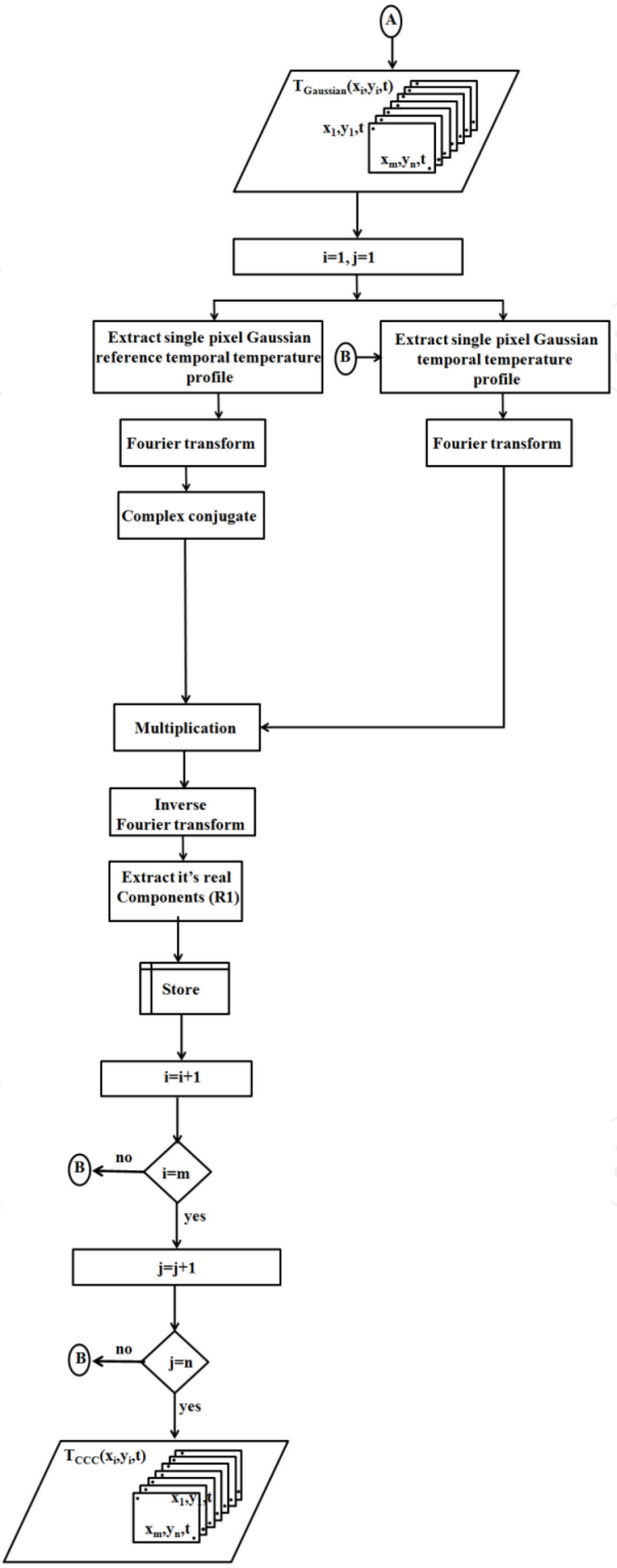

Figure 7.
Flow chart for obtaining pulse compression using circular correlation approach [19].

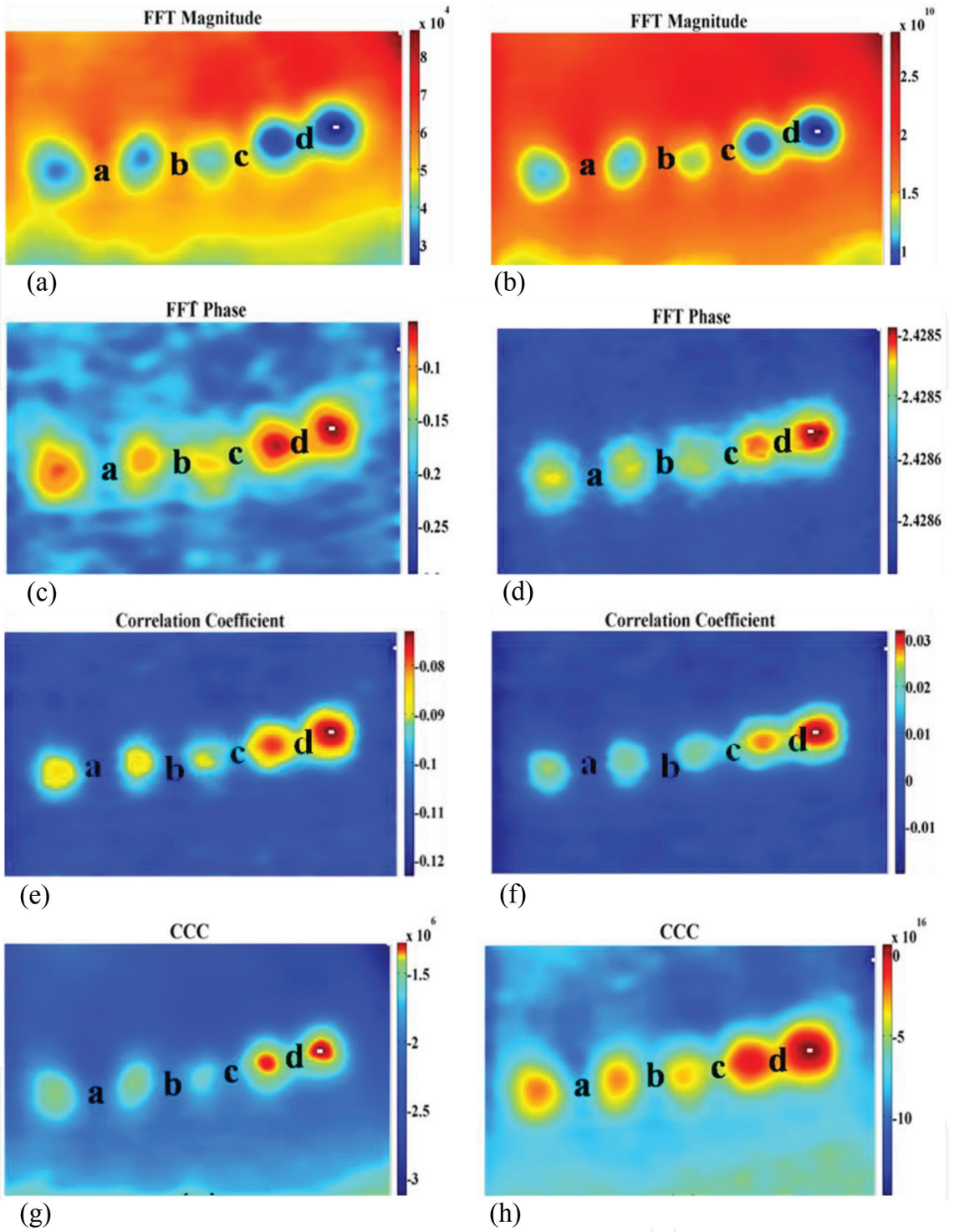

Figure 8.
Results obtained for frequency and time domain processing techniques. Frequency domain magnitude images obtained at a frequency of 0.02 Hz (a) using LFMTWI and (b) using GWFMTWI. Frequency domain phase image obtained (c) at a frequency of 0.06 Hz using LFMTWI and (d) at a frequency of 6.84 Hz using GWFMTWI. Correlation image obtained by cross correlation approach (e) at 62.92 s using LFMTWI and (f) at 46.32 s using GWFMTWI. Correlation images retrieved by circular correlation process at 56 s (g) using LFMTWI and (h) using GWFMTWI [19].

SNR is computed using formula as defined in (Eq. (14)) [13–19].

$$\boldsymbol{SNR} = 20Log\left(\frac{mean\ of\ defective\ area - mean\ of\ non\ defective\ area}{standarddeviation\ of\ non\ defective\ area}\right) \qquad (14)$$

Defect	FT Amp		FT phase		Linear correlation		CCC	
	LFM	GWFM	LFM	GWFM	LFM	GWFM	LFM	GWFM
a	29.84	34.83	19.93	19.69	35.10	40.67	31.57	34.55
b	34.11	37.65	34.83	21.44	40	43.51	34.22	38.03
c	34.85	39.30	36.41	24.28	44.85	46.24	35.16	39.86
d	40.56	43.98	42.38	26.66	49.72	49.45	39.11	43.51

Table 1.
Signal to noise ratio (in dB) for different grove cuts [19].

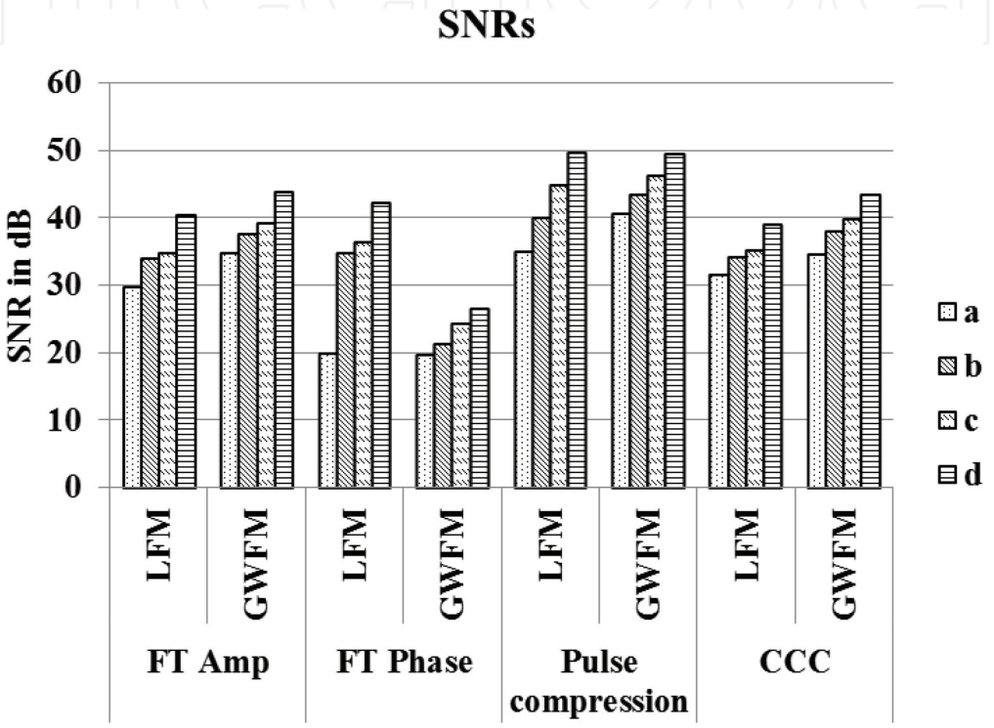

Figure 9.
Comparison of computed SNRs using different post-processing techniques for different grove cuts [19].

It is clear from **Table 1** and **Figure 9**, the results obtained using pulse compression approach shows better detection capabilities with GWFMTWI technique due to its inherent energy localization in time than that of the LFMTWI technique.

5. Conclusions

This present chapter highlights the capability of GWFMTWI technique to improve the corrosion detection capabilities of LFMTWI. Further results obtained from various multi-transform techniques in time and frequency domains are compared by considering the signal to noise ratio as a figure of merit. It clearly indicates that the GWFMTWI provides better detection performance in almost all the magnitude/correlation coefficient related data processing schemes over the conventional phase based data processing approaches. This chapter further highlights the importance of magnitude based processing approaches than that of widely used conventional frequency domain phase based approach for monitoring rebar corrosion in concrete structures.

Acknowledgements

This work was supported by the Science & Engineering Research Board (SERB), Department of Science and Technology, Govt. of India under Grant [number SB/S3/EECE/089/2014 dated 02-06-2014], and also partially supported by Aeronautics Research and Development Board (AR&DB), Govt. of India, under Grant no. DRDO/08/2031732/M/I dated 29.05.2014.

Conflict of interest

Authors have no conflict of interest.

Author details

Ravibabu Mulaveesala*, Geetika Dua and Vanita Arora
Department of Electrical Engineering, Indian Institute of Technology Ropar, Rupnagar, Punjab, India

*Address all correspondence to: ravibabucareiitd@yahoo.co.in

References

[1] Hellier C. Handbook of Nondestructive Evaluation. 2nd ed. USA: McGraw-Hill Professional Publishing; 2001

[2] Maldague X. Theory and Practice of Infrared Thermography for Nondestructive Testing. New York: Wiley; 2001

[3] Almond DP, Patel P. Photothermal Science and Techniques. Chapman and Hall Publication; 1996

[4] Mandelis A. Diffusion-Wave Fields: Mathematical Methods and Green Functions. New York: Springer; 2001

[5] Ringermacher HI, Howard DR, Filkins RJ. Flash-quenching for high resolution thermal depth imaging. Review of Progress in Quantitative Nondestructive Evaluation. 2004;**23**: 477-481

[6] Tam AC, Sullivan B. Remote sensing applications of pulsed photothermal radiometry. Applied Physics Letters. 2002;**43**:333-335

[7] Sakagami T, Kubo S. Applications of pulse heating thermography and lock-in thermography to quantitative non-destructive evaluations. Infrared Physics and Technology. 2002;**43**: 211-218

[8] Shepard SM. Introduction to active thermography for non-destructive evaluation. Anti-Corrosion Methods and Materials. 1997;**44**:236-239

[9] Almond DP, Lau SK. Defect sizing by transient thermography I: An analytical treatment. Journal of Physics D: Applied Physics. 1994;**27**:1063-1069

[10] Busse G, Wu D, Karpen W. Thermal wave imaging with phase sensitive modulated thermography. Journal of Applied Physics. 1992;**71**:3962-3965

[11] Maldague X, Galmiche F, Ziadi A. Advances in pulsed phase thermography. Infrared Physics and Technology. 2002;**43**:175-181

[12] Pickering S, Almond D. Matched excitation energy comparison of the pulse and lock-in thermography NDE techniques. NDT and E International. 2008;**41**:501-509

[13] Ghali VS, Mulaveesala R, Takei M. Frequency-modulated thermal wave imaging for non-destructive testing of carbon fiber-reinforced plastic materials. Measurement Science and Technology. 2011;**22**. art. no. 104018

[14] Mulaveesala R, Tuli S. Theory of frequency modulated thermal wave imaging for non-destructive sub-surface defect detection. Applied Physics Letters. 2006;**89**. art. no. 191913

[15] Ghali VS, Jonnalagadda N, Mulaveesala R. Three-dimensional pulse compression for infrared nondestructive testing. IEEE Sensors Journal. 2009;**9**: 832-833

[16] Tabatabaei N, Mandelis A. Thermal-wave radar: A novel subsurface imaging modality with extended depth-resolution dynamic range. Review of Scientific Instruments. 2009;**80**. art. no. 034902

[17] Ghali VS, Mulaveesala R. Comparative data processing approaches for thermal wave imaging techniques for non-destructive testing. Sensing and Imaging. 2011;**12**:15-33

[18] Mulaveesala R, Panda SSB, Mude RN, Amarnath M. Non-destructive evaluation of concrete structures by non-stationary thermalwave imaging.

Progress in Electromagnetics Research Letters. 2012;**32**:39-48

[19] Dua G, Mulaveesala R. Thermal wave imaging for non-destructive testing and evaluation of reinforced concrete structures. Insight: Non-Destructive Testing & Condition Monitoring. 2018;**60**(5):252-256

[20] Mulaveesala R, Siddiqui J, Arora V, Dua G, Subbarao GV, Muniyappa A. Testing and evaluation of concrete structures by thermal wave imaging. Proceedings of SPIE - The International Society for Optical Engineering. 2015; **9485**. art. no. 94850G

[21] Mulaveesala R, Panda SSB, Mude RN, Amarnath M. Nondestructive evaluation of concrete structures by nonstationary thermal wave imaging. Proceedings of SPIE - The International Society for Optical Engineering. 2012; **8354**. art. no. 83540B